Sub-size fracture testing of FY sea ice

C.A. Totman, O.E. Uzorka, J.P. Dempsey
Clarkson University, Potsdam, USA

D.M. Cole
US Army ERDC-CRREL, Hanover, USA

ABSTRACT: In the Fall of 2004, a total of 14 sea ice beams were harvested off the coast of Antarctica in McMurdo Sound to be used for lab-scale ice fracture testing at Clarkson University. A sub-size test program was initiated, with a view to developing a lab-scale ice fracture test methodology for first-year sea ice and to compare the results with large-scale in-situ experiments. The geometry chosen for the lab-scale experiments was the single-edge-notched, self-weight compensated beam (SENB-SWC) loaded in the three-point bend configuration (as per the Level II method described in the ACI Committee 446 report on "Fracture Toughness Testing of Concrete"). Closed loop, constant CMOD rate control was used to achieve stable crack growth during the experiment. Although it was difficult to achieve stable crack growth in these experiments, recent success suggests that the sub-size testing program under way will be successful.

1 INTRODUCTION

1.1 *Background*

The need for an accurate and reliable testing methodology to measure and characterize the fracture properties of ice is of great importance, but difficult to realize considering the range of experiments performed and the variability found in the results of these experiments. In-situ testing, though extremely important and necessary, is laborious, difficult and expensive. It is therefore desirable to develop an acceptable lab-scale test method so that a more systematic approach can be taken to acquire the fracture properties of ice. This information can then be used to more accurately develop and validate ice fracture models.

A rigorous instructional laboratory testing component was added to a fracture class taught at Clarkson University, Totman & Dempsey (2003), based on the ACI Committee 446 report on "Fracture Toughness Testing of Concrete." The results from the tests conducted by the students were very encouraging and it seemed a logical step to apply the test method to the fracture testing of ice. The Level II procedure described in the ACI 446 report was selected for the fracture testing of ice to establish its applicability. This procedure uses a single-edge-notched beam that is self-weight compensated (SENB-SWC) in the three-point bend configuration. Closed loop, constant rate crack mouth opening displacement (CMOD) control is used to load the specimen. By using CMOD control, the rate of crack opening is constant throughout the test and thus eliminates the variation in CMOD opening rate inherent with other loading methods. This is a very important aspect since the effect of loading rate is a critical parameter in the testing of ice.

Several initial experiments were performed using freshwater ice beams grown and harvested from an ice sheet in a basin situated in a cold room at Clarkson University. The results of the initial experiments showed that the test method was indeed suitable for ice. In the fall of 2004, a total of 14 first-year sea ice beams harvested off the coast of Antarctica in McMurdo Sound were shipped back to Clarkson for testing.

This paper assumes that the fracture of sea ice can be described by a cohesive or fictitious crack model (Hillerborg 1985, Mulmule & Dempsey 1997, 1999). The Level II method in the ACI 446 Report (2002) is followed, although the cohesive stress versus crack opening curve does not have the same characteristics as for concrete (Dempsey et al. 1999).

1.2 *Experimental Setup*

The Level II ACI 446 method was used as a general guideline for the lab scale sea ice fracture experiments, however, some modifications were made based on the first few experiments. The general arrangement is shown in Figure 1. The beams were cut oversize from the ice sheet in the field using a chainsaw and further cut to the proper size using a band

saw. The typical size of the beams was 150 mm x 150 mm x 950 mm. The loading span used for the experiments was 450 mm. This results in a span-to-depth ratio (S/D) of 3. The overall length of the beam is 50 mm longer than twice the span to ensure the weight of the beam does not contribute to loading. The notch in the beam is centrally located and cut with a radial arm saw such that the initial notch length (a_o) is ½ the beam depth. After cutting the notch, it is then sharpened by using the corner of a razor-type tool to initiate microcracks at the notch tip (DeFranco et al. 1991, Wei et al. 1991).

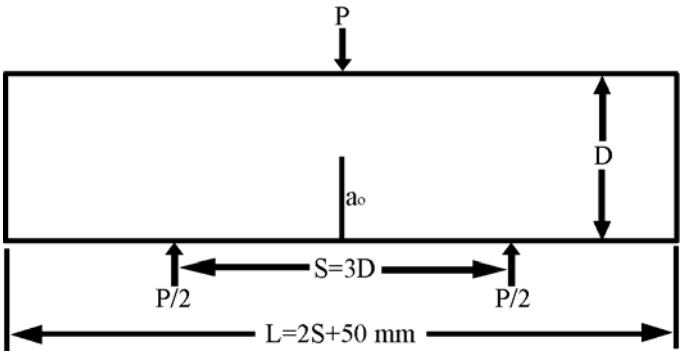

Figure 1. Three-point-bend SENB-SWC.

A total of 13 LVDTs and one load cell were used to measure displacements and load during the experiment. Figures 2 and 3 show the arrangement of the transducers attached to the sea ice beam. Both sides of the beam have an identical arrangement of instruments. Two ranges of LVDTs were attached to the bottom of the beam and both are used for CMOD control during the test. This was found to be necessary since the larger range LVDT did not provide suitable resolution for stable crack growth just before and after the peak load. A shorter range LVDT was used for control until the peak load occurs, at which time control is switched electronically to the longer range LVDT for the remainder of the test.

The four load point displacement (LPD) gages, two on each side of the beam, also have a coarse and fine range so that small events around the peak load region do not go unnoticed. The LPD gages are mounted to the specimen by means of a reference frame that is supported by the beam directly above the lower reaction supports. This ensures that any deformation at the supports is not measured by the LPD gages. One additional LPD gage is mounted to the frame of the test machine to compare with the LPD gages mounted on the reference frame.

Six more LVDTs are used to monitor the crack opening displacement (COD) and displacements ahead of the pre-cut notch, so-called fictitious crack (F) gages. These gages provide a means to measure the crack propagation and cohesive zone during the test.

The bend fixture used in this experiment was designed and fabricated at Clarkson University and is very robust such that the compliance of the fixture is insignificant compared to the sea ice. The lower reaction support rollers are mounted to the bend fixture using roller bearings to minimize friction effects at the supports. Rigid bearing blocks are placed between the sea ice beam and the rollers so that crushing or melting at the supports do not inhibit the rotation of the rollers. One lower support and the upper fixture are free to rotate parallel to the long axis of the beam to reduce torsional effects due to any minor geometric misfits. Four springs were attached from the center point-loading fixture to the beam in order to maintain good contact throughout the experiment. The test machine used for the experiments was an Instron 8500 series, 250 kN capacity servo-hydraulic load frame that provides good response and rigidity.

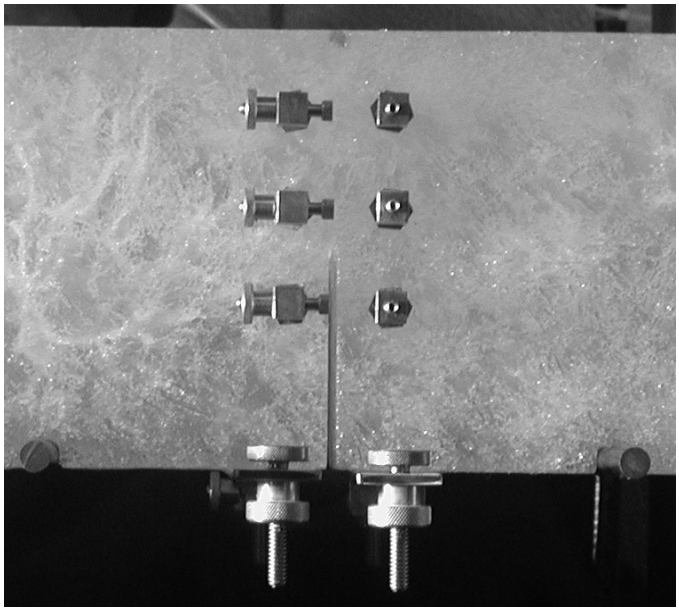

Figure 2:. Detail of gage mounting locations.

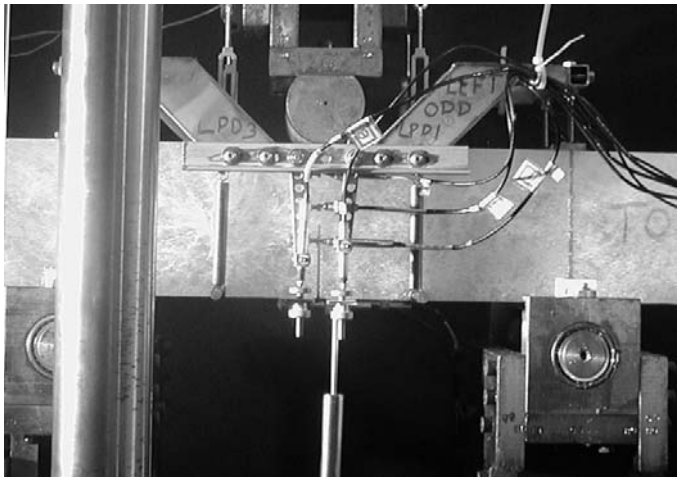

Figure 3. SENB-SWC transducer configuration.

1.3 *Data Acquisition and Control*

Sampling of each analog transducer channel during the tests was performed using 16-bit National In-

struments data acquisition hardware. The scan rate on each channel was 1000 samples per second, which was sufficient to fully characterize the peak load region as discussed in the results section.

Closed-loop feedback control of the CMOD was performed using an Instron 8800 series digital controller. The controller features a minimum control loop update rate of 250 microseconds, user selectable filters on all input channels and programmable control mode transfer. The high performance of this controller made it possible to obtain very tight control throughout the tests and maintain the constant CMOD rate. The bumpless, automatic control mode transfer capability of this controller made it possible to achieve a constant CMOD rate without interruptions for the duration of the experiment. As mentioned above, the key to success was using a high resolution, short range LVDT to control the CMOD rate until just after the peak load and then switching control to a longer range LVDT for the rest of the test.

Selecting appropriate tuning parameters for each feedback loop proved to be a difficult aspect of these experiments. Tuning was initially performed using the beam specimens with the pre-cut notch and the intact ligament. However, it was found, through trial and error that this resulted in a control system that overreacted to small fracture events. Since the compliance of the specimen decreases constantly throughout the test and changes drastically as the crack begins to propagate, it was observed that the control system would actually close the CMOD when crack propagation occurred and sometimes go into a resonance condition. Figure 4 shows a sample test result due to an under-damped control system.

To avoid the oscillations associated with an under-damped system, control loop tuning was performed on a beam that had been tested and the ligament fractured. To all intents and purposes, the self-weight compensation, springs and a small cohesive stress were holding the tuning specimen together. This resulted in tuning parameters that produced the proper level of damping for the specimen compliance. The outcome of this tuning method (shown in Fig. 5) was a stable, constant rate CMOD throughout the bend test. Unfortunately, overcoming this tuning issue consumed about half of the sea ice beams shipped back from Antarctica. Moreover, since stable fracture had been achieved, the displacements on subsequent tests exceeded initial estimates such that the displacement transducers were going out of range before the conclusion of the test. This led to a few more experiments with incomplete data and even fewer beams to work with. Longer range LVDTs were fitted to the setup in an effort to capture the complete unloading behavior.

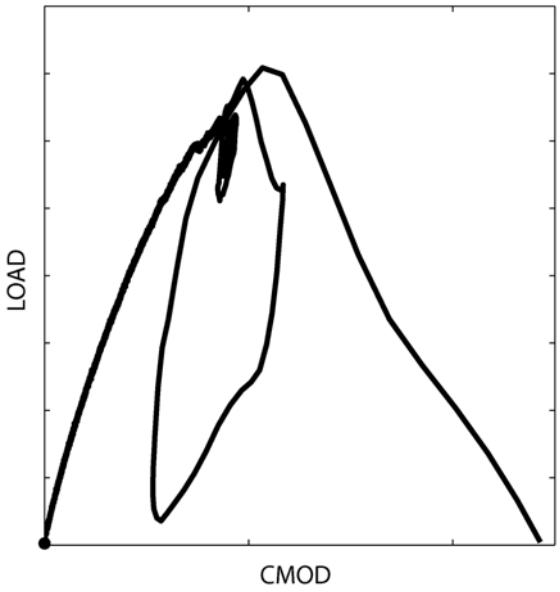

Figure 4. Result of tuning on a notched beam with intact ligament.

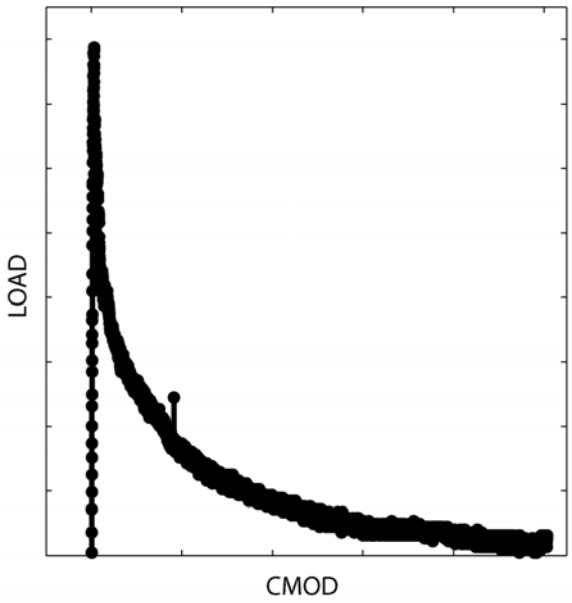

Figure 5. Result of tuning on a pre-tested beam.

2 RESULTS & CALCULATIONS

2.1 *Discussion*

The full analysis of this set of experiments is still in progress but some of the initial calculations and results will be presented here. All the experiments were run at a constant CMOD rate of 10 microns per second and isothermal temperature of –2.5ºC. The temperature of each beam was monitored using thermocouples near the surface and at the core of the beam. Following each experiment, salinity and density measurements were taken. Thin sections of each specimen were obtained and photographed to determine grain size distribution and the extent and direction of crystallographic alignment. Additionally, post-test photographs were taken of thin sections of

the fracture profile to conduct a fractal analysis of the fracture surfaces.

2.2 *Work of Fracture and Fracture Energy*

The measured work of fracture (W_{Fm}) is calculated as the area under the load versus LPD record. Typical results of the successful tests are shown in Figures 6-8. The area was computed using trapezoidal approximation directly from the data. As per the ACI Committee 446 report, the residual load at the end of the test is subtracted from the complete load record when determining the work of fracture. For these tests this value ranged from 60 to 90 Newtons at 10 mm CMOD. .

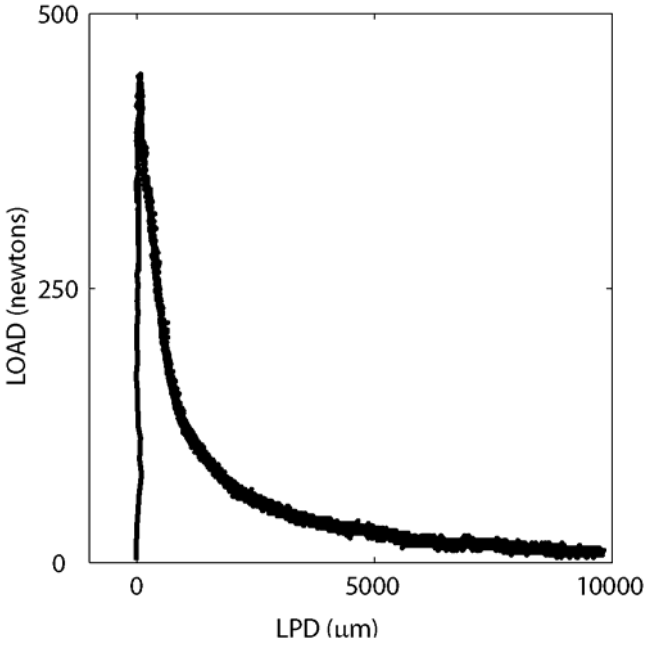

Figure 6. Specimen 4B measured work of fracture with residual load subtracted.

Some specimens did not completely fracture, as illustrated in Figure 9 where a post-test view of the beam is shown after 10 mm CMOD. Clearly, more experiments need to be conducted to capture the complete unloading.

Following directly from the ACI Committee 446 Report, once the W_{Fm} is determined from the load versus LPD record the total work of fracture, W_F, is estimated based on the behavior of the far tail region of the load-CMOD record. The corrected load, P_1, is found by subtracting the residual load at the end of the test from all points in the measure load record. The quantity X is computed from the CMOD record, according to Equation 1, corresponding to all points in the post peak P_1 record that are less than or equal to 5% of the corrected peak load. The far tail constant, A, is then found by least squares fitting of the quadratic equation in Equation 2. The far tail constant is then used in Equation 3 to compute the total work of fracture. Finally, the fracture energy, G_F, is found from Equation 4. Work of fracture and fracture energy results for two of the most successful and complete experiments are summarized in Table 1.

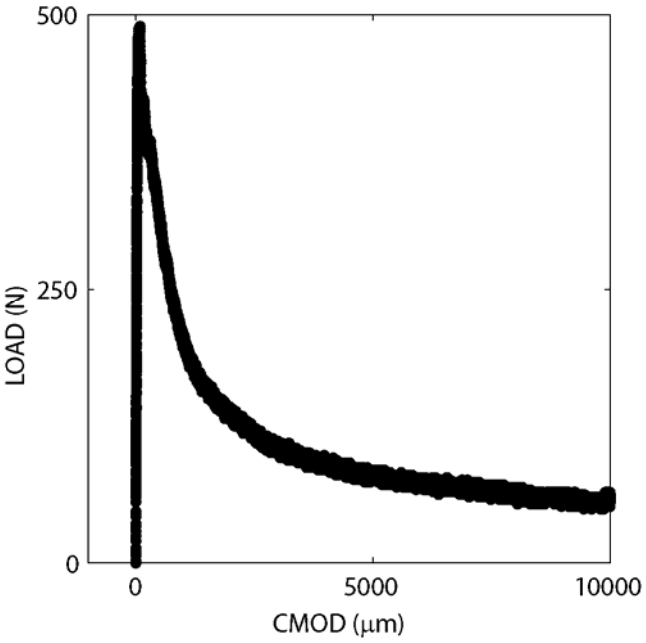

Figure 7. Specimen 4B record of load vs. CMOD showing residual load.

It should be noted that the sea ice used in these experiments was very highly drained and may not be representative of the in-situ conditions. The cold storage facility at Clarkson was not in an operational state at the time the beams arrived from Antarctica and, as such, the ice was stored in the same cold rooms that the preparation and testing were conducted.

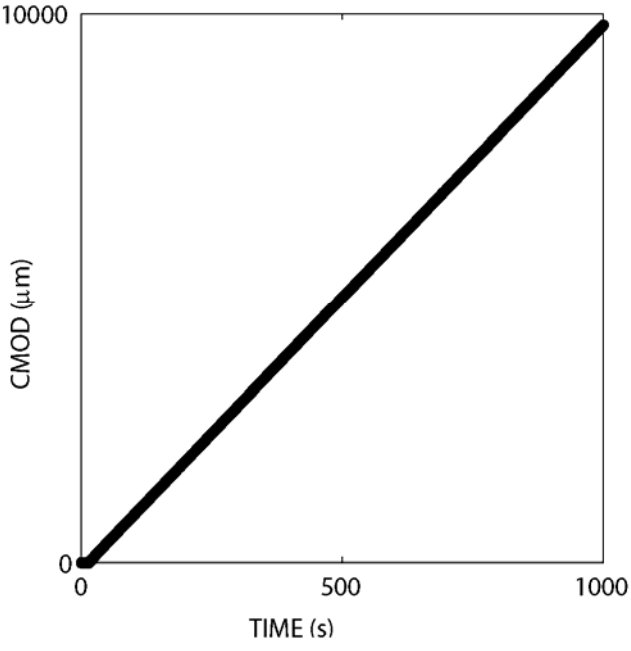

Figure 8. Specimen 4B record of constant CMOD rate control.

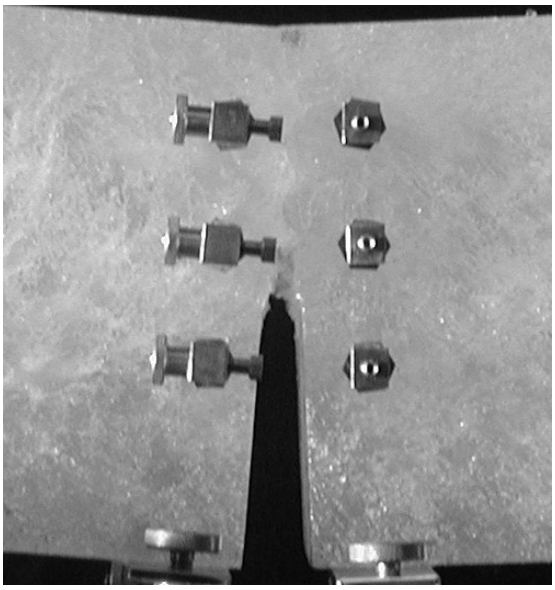

Figure 9. Fracture after 10 mm CMOD illustrating the extent of bridging.

The cold rooms where kept at approximately –7ºC except when testing was conducted and the temperature adjusted to –2.5ºC. The storage conditions and time spent in storage resulted in specimens that were highly drained with low salinity and density values. Large continuous and discontinuous drainage channels were present throughout the sea ice beams.

Another factor affecting the results was the design of the reaction support rollers. As mention previously, they are mounted on roller bearings to minimize friction. However, this particular fixture was designed for use with concrete at room temperature and the bearings did not perform as well in the subfreezing test conditions. A new fixture is currently being designed and fabricated at Clarkson specifically for conducting the ice fracture tests that will eliminate this issue.

2.3 *Peak Load Region Fracture Behavior*

From the test records shown in Figures 6 & 7, the fracture behavior of the first year sea ice at a relatively warm temperature appears to exhibit a brittle behavior followed by an extensive region of diminishing cohesive stress. However, if the peak load region is shown in greater detail using the load and the short-range CMOD gage, Figure 10, the fracture events can be characterized by a series of stress releases. Figure 11 is the same experiment showing the load and the short range LPD and Figure 12 shows the short range CMOD gage versus time to verify that the fracture events were not due to deviations in CMOD control.

It is well known that ice can exhibit a large and complex damage zone before a dominant fracture path develops. However, even when there exists a fracture path, it may not be exclusive. There is extensive bridging that occurs and the COD must be relatively large before the critical opening is reached and the cohesive stress diminishes to zero. Figure 13 shows the load versus time record around the peak load region to give a sense of the rate of energy release. The load drops are sudden with very little change in separation, which suggests only small, hairline cracks developed through the ligament in the more brittle phases of the ice microstructure. Moreover, since the stress releases are followed by a rise in the load before another release, the small cracks that have developed are not continuous. The coalescence of these small cracks occurs a short time later when there is sufficient separation such that a more dominant fracture path develops. Following the development of the initial, major crack, the process zone continues to grow and the dominant crack continues to advance in a stable manor.

$$X = \frac{1}{\left(w_M - w_{MA}\right)^2} - \frac{1}{\left(w_{MR} - w_{MA}\right)^2} \qquad (1)$$

Where w_M = recorded CMOD, w_{MA} = CMOD at zero P_1 for the rising part of the curve, w_{MR} = CMOD at the end of test.

$$P_1 = X(A + KX) \qquad (2)$$

Where P_1 = corrected load, A = far tail constant, K = unused coefficient.

$$W_F = W_{Fm} + \frac{2A}{\delta_R - \delta_A}\left(\frac{S}{4D}\right)^2 \qquad (3)$$

Where W_F = total work of fracture, W_{Fm} = measured work of fracture, δ_R = LPD at end of test, δ_A = LPD at zero P_1 for the rising part of the curve, S = reaction support span, D = beam depth.

$$G_F = \frac{W_F}{Bb} \qquad (4)$$

Where G_F = fracture energy, W_F = total work of fracture, B = beam thickness, b = uncracked ligament length.

Table 1. Summary of test results.

Specimen ID	W_F (J)	G_F (N/m)
4B	0.350	37
5B	0.379	39

Further information concerning crack propagation can be gathered from the load versus displacement records of the F gages located ahead of the precut notch. Using simple beam theory and taking the neutral axis to be half the length of the uncracked ligament, the first gage ahead of the notch, F1, is positioned below the neutral axis in the tensile region. The next gage, on the same side of the beam, F3, is located above the initial neutral axis in the compressive region. Figures 14 and 15 show the record of the F1 and F3 gages, respectively.

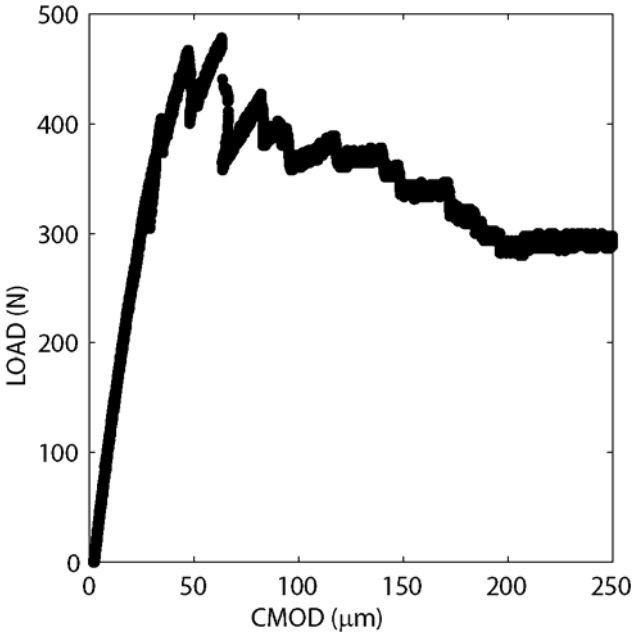

Figure 10. Short range CMOD gage record to illustrate the fracture behavior in the peak load region.

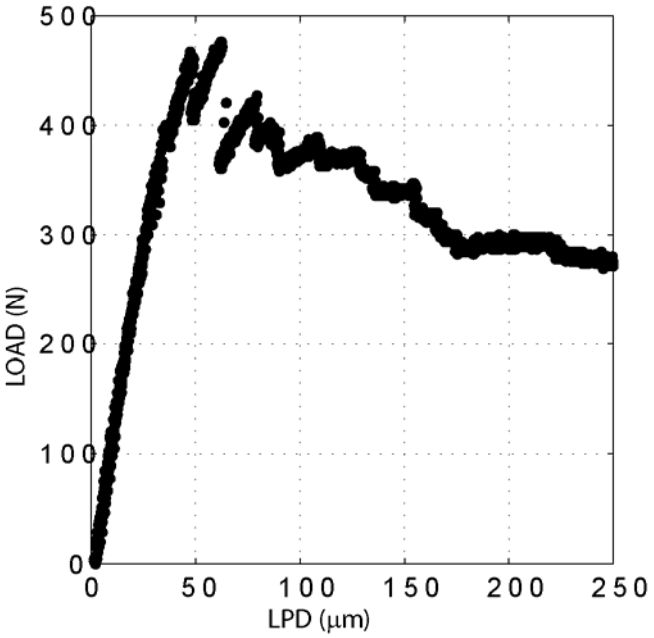

Figure 11. Record of short range LPD to verify the fracture behavior.

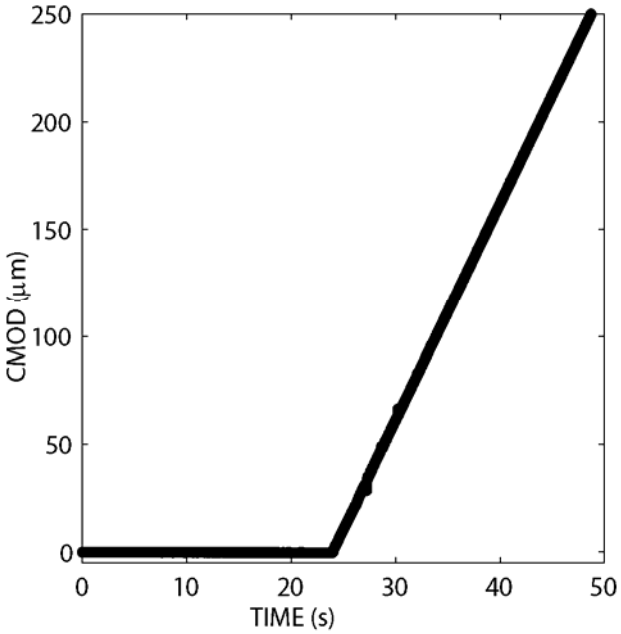

Figure 12. CMOD vs. time record to show constant rate control in the peak load region.

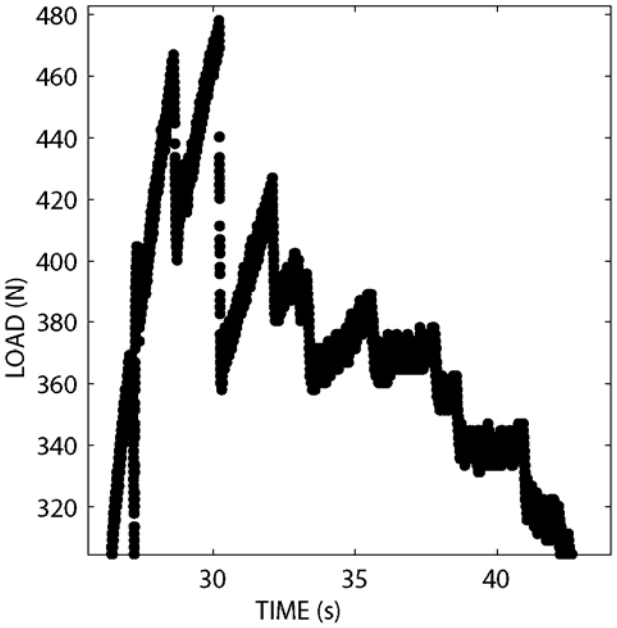

Figure 13: Load vs. time record in the peak load region.

Observing the record of the F1 gage, located in the tensile region of the ligament, it exhibits similar behavior as the CMOD, as would be expected. However, the F3 gage, in the initial compressive region, shows a quite different response. From zero to the peak load, the separation closed a few microns confirming this region of the ligament was in compression until the peak load is reached and the crack begins to advance. Moreover the "spiky" behavior is absent and there is simply one dominant separation that occurs before the fracture activity transitions to a cohesive dominated failure.

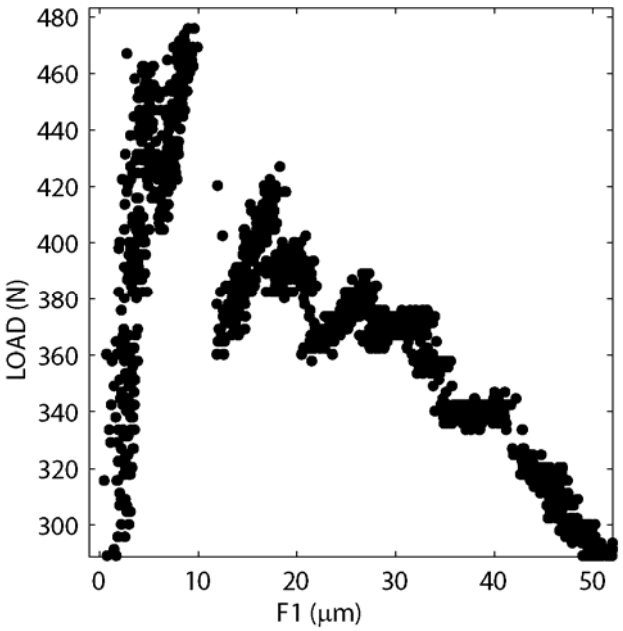

Figure 14. F1 gage located below the initial neutral axis in the tensile region.

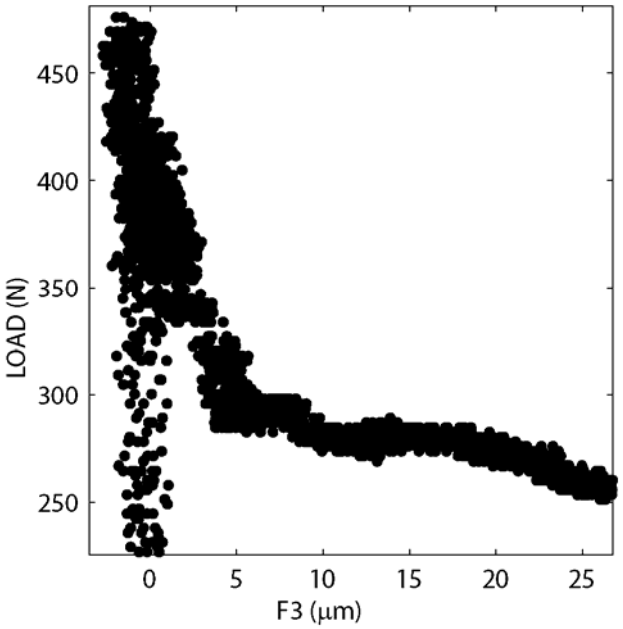

Figure 15. F3 gage located above the pre-tested beam's neutral axis in the initial compressive region of the ligament.

From these results it can be concluded that numerous small cracks developed at different locations in the fracture process zone before coalescing into a dominant failure path. At this time, the main crack was then able to advance ahead of the F3 gage location transitioning the stress in this region from compressive to tensile.

3 CONCLUSIONS

The outcome of the initial round of fracture testing of sea ice beams using the Level II method described in the ACI Committee 446 report has yielded successful results warranting further testing and detailed analysis. The SENB-SWC geometry along with CMOD control provides an effective means to characterize the fracture behavior and extract relevant fracture properties of the sea ice.

A more thorough and controlled round of testing is scheduled to begin in the spring of 2007 when 40 first-year sea ice beams will arrive. These beams were harvested off the coast of Antarctica in McMurdo Sound during a round of in-situ testing conducted during the fall of 2006.

Since the first series of sea ice beam tests, the cold storage room has been repaired so that the beams can be stored at a constant –20ºC until testing. Fabrication of a custom bend fixture designed specifically for ice testing is underway so that unwanted external influences on the results will be eliminated. The first series of tests reported here provided numerous lessons and insights that will be applied to the incoming test program so that the testing will be more efficient and productive.

Ongoing application of the cohesive crack model to the in-situ Antarctic sea ice tests is able to track the stable growth of the crack and back-calculate associated changes to the stress separation curve, the fracture energy and the process zone size. The fracture energy determined from the in-situ tests is an increasing function with extent of stable crack growth. The values determined to date are approximately a third of the values reported in Table 1. Unfortunately, the in-situ ice and the ice finally tested at Clarkson University differed considerably in composition, salinity and porosity. With better control of the temperature history, and the custom bend fixture, it will be interesting to see if the values become more compatible.

ACKNOWLEDGEMENT

The financial support of the US National Science Foundation through the Antarctic Oceans and Climate Systems Program, Award # 0338226 and the Division of Undergraduate Education, Award # 0311075 is gratefully acknowledged.

REFERENCES

ACI Committee 446 Report 2002. *Fracture Toughness Testing of Concrete.*

DeFranco, S.J., Wei, Y. & Dempsey, J.P. 1991 Notch-acuity effects on the fracture toughness of saline ice. *Annals of Glaciology* Vol. 15: 230-235.

Dempsey, J.P., Adamson, R.M. & Mulmule, S.V. 1999. Scale effects on the in-situ tensile strength and fracture of ice. Part II: First-year sea ice at Resolute, N.W.T. *Int. J. Fract.* 95: 347-366

Hillerborg, A. 1985. The theoretical basis of a method to determine the fracture energy G_F of concrete. Materials and Structures 18: 291-296.

Mulmule, S.V. & Dempsey, J.P. 1997. Stress-separation curves for saline ice using the fictitious crack model. *ASCE J. Eng. Mech.* 123: 870-877

Mulmule, S.V. & Dempsey, J.P. 1998. A viscoelastic fictitious crack model for the fracture of sea ice. *Mech. Time-Dependent Materials* 1: 331-356

Totman, C.A. & Dempsey, J.P. 2003. Design of concrete fracture experiments. *Proceedings ASEE Annual Conference* Paper # 2215, 8p (in CD ROM)

Wei, Y., DeFranco, S.J. and Dempsey, J.P. 1991. Crack fabrication techniques and their effects on the fracture toughness and CTOD for freshwater columnar ice. J. Glaciology 37: 270-280